Human USP18 deficiency underlies type 1 interferonopathy leading to severe pseudo-TORCH syndrome

Human USP18 deficiency underlies type 1 interferonopathy leading to severe pseudo-TORCH syndrome

Marije E.C. Meuwissen,[1]* Rachel Schot,[1]* Sofija Buta,[8,9,10] Grétel Oudesluijs,[1] Sigrid Tinschert,[11,12] Scott D. Speer,[8,9,10] Zhi Li,[13] Leontine van Unen,[1] Daphne Heijsman,[2] Tobias Goldmann,[8] Maarten H. Lequin,[3] Johan M. Kros,[4] Wendy Stam,[1] Mark Hermann,[8,9,10] Rob Willemsen,[1] Rutger W.W. Brouwer,[5] Wilfred F.J. Van IJcken,[5] Marta Martin-Fernandez,[8,9,10] Irenaeus de Coo,[6] Jeroen Dudink,[7] Femke A.T. de Vries,[1] Aida Bertoli Avella,[1] Marco Prinz,[14] Yanick J. Crow,[15,16] Frans W. Verheijen,[1]* Sandra Pellegrini,[13]* Dusan Bogunovic,[8,9,10]** and Grazia M.S. Mancini[1]**

[1]Department of Clinical Genetics, [2]Department of Bioinformatics, [3]Department of Radiology, [4]Department of Pathology, [5]Erasmus Center for Biomics, [6]Department of Child Neurology, and [7]Department of Neonatology, Erasmus University Medical Center, 3015 CE Rotterdam, the Netherlands
[8]Department of Microbiology, [9]Department of Pediatrics, and [10]The Mindich Child Health and Development Institute, Icahn School of Medicine at Mount Sinai, New York, NY 10029
[11]Medical Faculty Carl Gustav Carus, Technical University of Dresden, 01069 Dresden, Germany
[12]Division of Human Genetics, Medical University Innsbruck, 6020 Innsbruck, Austria
[13]Institut Pasteur, Cytokine Signaling Unit, Centre National de la Recherche Scientifique URA 1961, INSERM U 1221, 75724, Paris, France
[14]Institute of Neuropathology and BIOSS Center for Biological Signaling Studies, University of Freiburg, 79085 Freiburg, Germany
[15]INSERM UMR 1163, Laboratory of Neurogenetics and Neuroinflammation, Imagine Institute, Necker Hospital, Paris Descartes University, 75015 Paris, France
[16]Manchester Centre for Genomic Medicine and Academic Health Science Centre, University of Manchester, Manchester M13 9PL, England, UK

Pseudo-TORCH syndrome (PTS) is characterized by microcephaly, enlarged ventricles, cerebral calcification, and, occasionally, by systemic features at birth resembling the sequelae of congenital infection but in the absence of an infectious agent. Genetic defects resulting in activation of type 1 interferon (IFN) responses have been documented to cause Aicardi-Goutières syndrome, which is a cause of PTS. Ubiquitin-specific peptidase 18 (USP18) is a key negative regulator of type I IFN signaling. In this study, we identified loss-of-function recessive mutations of *USP18* in five PTS patients from two unrelated families. Ex vivo brain autopsy material demonstrated innate immune inflammation with calcification and polymicrogyria. In vitro, patient fibroblasts displayed severely enhanced IFN-induced inflammation, which was completely rescued by lentiviral transduction of USP18. These findings add *USP18* deficiency to the list of genetic disorders collectively termed type I interferonopathies. Moreover, USP18 deficiency represents the first genetic disorder of PTS caused by dysregulation of the response to type I IFNs. Therapeutically, this places USP18 as a promising target not only for genetic but also acquired IFN-mediated CNS disorders.

Maternal exposure to microbial pathogens can cause severe fetal brain damage that is detectable at birth. The acronym TORCH (toxoplasmosis, other [syphilis, varicella, mumps, parvovirus and HIV], rubella, cytomegalovirus, and herpes simplex) was first coined to highlight the commonality of the observed phenotype secondary to transplacental transmission of such microbes (Shin et al., 1976; Fine and Arndt, 1985; Donley, 1993). Events involved in the control of infections are associated with important immune-mediated collateral damage, with the CNS being more susceptible due to its immune privileged status (Konradt and Hunter, 2015). CNS characteristics of TORCH include microcephaly, white matter disease, cerebral atrophy, and calcifications.

Children are considered to have pseudo-TORCH syndrome (PTS) if they display a clinical phenotype indicative of in utero exposure to infection, but where the disorder has a noninfectious etiology (Reardon et al., 1994; Vivarelli et al., 2001). The high frequency of consanguinity among families with PTS suggests that many cases are genetic, inherited as autosomal recessive traits (Vivarelli et al., 2001).

One known rare Mendelian mimic of congenital infection, overlapping with and falling under the umbrella of PTS, is the Aicardi-Goutières syndrome (AGS; OMIM #225750). AGS is genetically heterogeneous, caused by mutations in any of *TREX1*, *RNASEH2B*, *RNASEH2C*, *RNASEH2A*, *SAMHD1*, *ADAR1*, and *IFIH1* (Crow and Rehwinkel, 2009;

*M.E.C. Meuwissen, R. Schot, F.W. Verheijen, and S. Pellegrini contributed equally to this paper.

**D. Bogunovic and G.M.S. Mancini contributed equally to this paper.

Correspondence to Grazia M.S. Mancini: g.mancini@erasmusmc.nl; or Dusan Bogunovic: Dusan.Bogunovic@mssm.edu

M.E.C. Meuwissen's present address is Dept. of Medical Genetics, Antwerp University Hospital, 2650 Edegen, Belgium.

A. Bertoli Avella's present address is Centogene, 18057 Rostock, Germany

Abbreviations used: AGS, Aicardi-Goutières syndrome; C, control; H&E, hematoxylin and eosin; ISG, IFN-stimulated gene; P, patient; PTS, Pseudo-TORCH syndrome; TORCH, toxoplasmosis, other (infection), rubella, cytomegalovirus, herpes simpex virus.

The Rockefeller University Press $30.00
J. Exp. Med. 2016 Vol. 213 No. 7 1163–1174
www.jem.org/cgi/doi/10.1084/jem.20151529

Rice et al., 2012). AGS results from an aberrant accumulation/sensing of IFN-stimulatory nucleic acids, which are then misrepresented as viral/non-self by the innate immune machinery, leading to the persistent induction of type 1 IFN-mediated inflammation. Similar increases in type 1 IFN production have also been documented in genetic disorders in which other components of the IFN signaling pathway are constitutively activated (Crow and Casanova, 2014; Liu et al., 2014; Crow, 2015; Zhang et al., 2015). The genetic cause in most pseudo-TORCH syndrome patients, however, remains largely unknown.

Here, we identify a novel genetic etiology of a type 1 interferonopathy leading to severe PTS.

RESULTS AND DISCUSSION

Clinical characterization

We studied a Turkish consanguineous family (family A) with three children (patient 1 [P1], P2, and P3) affected by PTS with severe brain damage. We also analyzed a previously reported nonconsanguineous German family (family B) with two children (P4 and P5) affected by a similar disorder (Knoblauch et al., 2003; Fig. 1 A). Pre- and postnatal brain ultrasound and MRI scans showed an enlargement of lateral ventricles, calcifications, and hemorrhages (Fig. 1 B). Parents in both families are healthy and there was no medical indication to perform brain MRI scans.

In family A, the antenatal presentation of the condition in P1 led to a termination of pregnancy at 23 wk of gestation. In P2 and P3, presentation was neonatal and death occurred within two weeks. P2 and P3 had severe intracerebral hemorrhages and developed liver dysfunction, ascites, and lactic acidosis (Fig. 1 B, a–k). P2 also displayed severe thrombocytopenia with petechiae. Both siblings developed respiratory failure requiring ventilation, together with bradycardia, and they died at the ages of 7 and 17 d, respectively (see Supplemental Text for clinical details). Blood cells and cerebrospinal fluid were not available. In family B, two brothers (P4 and P5) presented a PTS-like phenotype with both neurological and systemic features, including thrombocytopenia, petechiae, ascites, hepatomegaly, and systemic calcifications, and were previously reported. (Knoblauch et al., 2003; Fig. 1 B, i). The clinical findings for both families are summarized in Table 1.

Identification of loss-of-function *USP18* mutations

We performed haplotype linkage analysis assuming the autosomal recessive inheritance of a homozygous mutation in family A. We demonstrated only one overlapping area of homozygosity among affected individuals, on chromosome 22q11.1-22q11.21, with a suggestive LOD score of 2.83 (Lander and Kruglyak, 1995) (Fig. 1 C). The linked region spans the markers rs5746398-rs5757914 (chr22:17929926 -22694656, GRCh37.p10) and contains 200 genes (Fig. 1 C and Fig. S1). Whole-exome sequencing failed to identify a putative pathogenic mutation, as the area was poorly covered (Tables S1 and S2). Capillary DNA sequencing of the missing exons in the linked region (Table S3) identified a homozygous mutation (c.652C>T) in the three patients that was present in the heterozygous state in the healthy brother and both parents (primers in Table S4). This variant mapped to exon 7 of the ubiquitin-specific protease 18 (*USP18)* gene (OMIM #607057) and was predicted to result in replacement of the glutamine 218 residue by a premature stop codon (p.Gln218X; Fig. 1 D). The variant was not found in 190 Turkish control chromosomes, or in the dbSNP or ExAC databases. Analysis of 952 DNA samples sequenced by Complete Genomics (CG; whole genome sequencing, containing 481 samples of Wellderly-aged Americans cohort, 46 public CG data from in-house database of the Erasmus Medical Center, and 425 samples from the 1,000 Genomes Project), which provide full coverage of *USP18*, showed no c.652C>T variant, thus indicating that this is an extremely rare variant (Fig. S2).

In family B, Sanger sequencing of *USP18* in P4 and P5 revealed the same mutation (c.652C>T) present in the heterozygous state (Fig. 1 D). Haplotype analysis of 86 SNPs on Illumina cyto-snp-850K-B arrays covering the 400-kb area across the *USP18* allele containing the c.652C>T change (chr 22: 18483880–18891398, hg19; *USP18* spans bp 18632666–18660164) revealed a shared c.652C>T allele between the two families, consistent with remote common ancestry (Table S5). Capillary DNA sequencing of *USP18* is laborious because of its high homology with the pseudogene *USP41* (Fig. S3). Genomic sequencing with *USP18*-specific primers did not detect a second mutation in family B. Quantitative RT-PCR of *USP18* mRNA in fibroblasts was performed using primers across exon 4 (forward) to exon 6 (reverse), before and after stimulation with IFN-β-1a (Fig. 1 E; primer sequences in Table S4). P1 and P2 showed low basal and induced transcript levels, whereas P4 and P5 showed an impaired induced transcript level. On the assumption of a cryptic mutation on the second allele in family B, we designed six different primer sets covering the whole cDNA (Fig. 2 A), including primers to amplify only the WT allele not carrying the c.652C>T mutation (marked with a red x in the schematic of Fig. 2 A) and performed RT-PCR.

RT-PCR amplifying exon 1–6 of *USP1*8 yielded the expected 782-bp product in the control (C1), the healthy heterozygote sibling of family A (Het FamA), and P4 of family B, consistent with an intact 5′ portion of the transcript. The lower intensity band detected in homozygous P1, from family A, was consistent with nonsense-mediated RNA decay (Fig. 2 B, product A). RT-PCR amplifying exon 6–9 of *USP18* yielded the expected 393-bp band in C1 and Het FamA, but a lower intensity band was detected in the homozygous P1, consistent with nonsense-mediated RNA decay. A normal product was detected in P4, consistent with heterozygosity at position c.652C>T (Fig. 2 B, product B). RT-PCR amplifying exon 6–11 of *USP18* yielded the expected 863-bp product in C1 and Het FamA. In P1, this band was of lower intensity, consistent with nonsense-mediated decay, but importantly, P4 yielded an even more diminished 863-bp

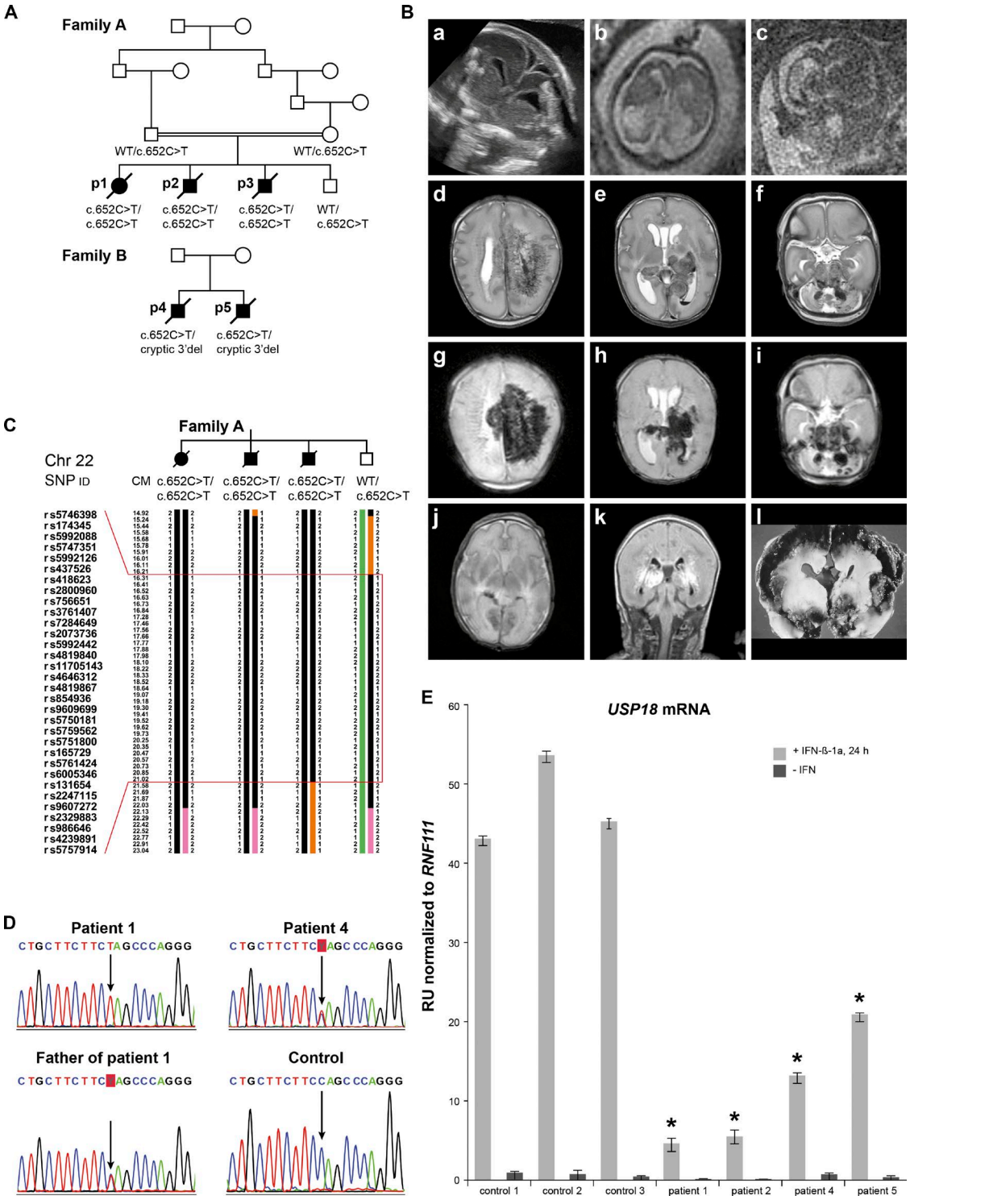

Figure 1. **Pedigrees, brain imaging, genomic, and expression data.** (A) Pedigrees of family A and B (p1, p2, p3, p4, and p5 indicate P1–P5). Family A includes three affected siblings (P1, P2, and P3) and one unaffected (heterozygote) sibling; family B includes two affected siblings (P4 and P5). The corresponding genotypes are indicated. (B) Prenatal ultrasound (22nd gestational week; a) and fetal MRI (b and c) for P1, showing ventriculomegaly with irregular ventricle linings, parenchymal lesions, and cortical destruction. (d–k) Postnatal MRI; d, e, and f (T2-weighted images) and g, h, and i (susceptibility-weighted images) concern P2, and show extensive parenchymal, basal ganglial, and cerebellar hemorrhages. j (T2 weighted) and k (FLAIR) are images of P3, showing bilateral thalamic hemorrhage and white matter hyperintensities. i depicts a postmortem brain analysis for P4, with massive hemorrhagic destruction. (C) Haplotype analysis of the linkage area on chromosome 22q in family A, including SNP IDs and location on the chromosome in centimorgans

product, consistent with nonsense-mediated decay from one allele (c.652T) and a cryptic mutation after exon 9, possibly affecting splicing (Fig. 2 B, product C).

RT-PCR amplifying only the WT c.652C allele was also performed (red cross in schematic of Fig. 2 A). Amplifying exon 1–7 yielded the expected 830-bp product in C1, Het FamA, and P4, consistent with an intact 5′ portion of the transcript. The product was essentially absent in the homozygous P1, consistent with primer mismatch (Fig. 2 B, product D). Amplifying exon 7–9 yielded the expected 321-bp product in P4, similar to C1 and Het FamA, and no product in P1, again as a result of primer mismatch (Fig. 2 B, product E).

Amplifying exons 7–11 yielded the expected 791-bp product in C1 and Het Fam A, no product in P1, consistent with primer mismatch, and no product in P4 consistent with a cryptic mutation on the second allele (Fig. 2 B, product F). These experiments confirmed the presence of an altered transcript in family B.

Additional sequencing of the introns between exon 9 and 11 did not show any new variant in family B (primers in Table S4). This excluded a splicing error as explanation for the altered transcript.

Finally, 3′ RACE PCR was performed. For the first PCR, 5′ primers starting in exon 6 up to the poly-A tail were designed. The resulting product was amplified by nested PCR using 5′ primers in exon 7, annealing only to the WT c.652C sequence (Fig. 2 A, amplicons G and H). This experiment revealed four different products in C1, Het FamA, P1, and P4 (Fig. 2 C, band 1–4). Upon sequencing, the 1,200-bp product (Fig. 2 C, band 1) corresponds to the WT sequence of *USP18* and is present in C1 and Het FamA, but is not detectable in P4. A 1,000-bp product (Fig. 2 C, band 2) is only present in P1. This product corresponds to an alternative transcript of *USP41* fused with a part of the 3′ distal gene *LOC105372866*, a result of biallelic primer mismatch with the nested primer in *USP18*. An 850-bp product (Fig. 2 C, band 3) is present in C1, Het FamA, P1, and P4 and corresponds to an alternative transcript of *USP41*. A product of ∼800 bp is exclusively present in P4 (Fig. 2 C, band 4). Capillary sequencing of this product shows a repeat-rich sequence that maps distal to the 3′ UTR region of *USP18*, suggestive of a large deletion at the 3′ end of *USP18* as the second mutation in family B (cryptic 3′ deletion).

Western blot analysis of lysates prepared from skin fibroblasts, with and without IFN-β stimulation, using monoclonal antibodies against the N-terminal part of USP18, revealed a complete lack of USP18 protein in the patients from both family A and B in contrast to healthy controls (Fig. 2 D). These results indicate that both the c.652C>T and the cryptic 3′ deletion in *USP18* alleles produce no or abnormal transcripts, respectively, which are not translated into normal USP18 protein. Altogether these genomic, genetic, molecular, and biochemical analyses lead us to conclude that the complete USP18 deficiency results from autosomal recessive homozygous *USP18* mutations in family A and from compound heterozygous mutations in family B.

USP18 is a type 1 IFN-stimulated gene (ISG) that encodes a protein that exerts dual functions: regulatory and enzymatic. USP18 is a negative feedback regulator of type I IFN signaling (Malakhova et al., 2006). USP18 is also an isopeptidase that cleaves the ubiquitin-like ISG15 protein from conjugated proteins (Zhang and Zhang, 2011). The study of *Usp18*$^{-/-}$ mice highlighted a role of USP18 in the CNS. Yet, the *Usp18*$^{-/-}$ phenotype appears to be dependent on the genetic background of mice. In the fully backcrossed FVB/N background, a majority of *Usp18*$^{-/-}$ mice were reported to have a normal lifespan, in the C57BL/6 background *Usp18*$^{-/-}$ mice died before E15.5, and in a mixed C57B/L6 × 129/Sv background they reached birth and showed an intermediate phenotype (Zhang and Zhang, 2011). All mice displayed varying degrees of neurological signs and brain inflammation, suggesting that the lack of USP18 has an impact on the CNS that differs in severity depending on the background (Ritchie et al., 2002; Goldmann et al., 2015). These CNS alterations were reminiscent of the sequelae of viral infection (Ritchie et al., 2002). Importantly, none of these diverse murine phenotypes were recognized as potential mimics of the human pseudo-TORCH syndrome.

Patient brain pathology and activation of innate immune response

In vivo brain imaging in USP18-deficient patients mostly showed severe hemorrhage, with findings reminiscent of those in other cases of perinatal hemorrhage, such as genetic porencephaly caused by *COL4A1* and *COL4A2* mutations (Meuwissen et al., 2015). Genetic testing in a cohort of 38 patients with isolated prenatal or infantile cerebral hemorrhage, where *COL4A1* and *COL4A2* mutations had been excluded, failed to identify additional *USP18* mutations. We therefore deduce that *USP18* mutations are infrequent.

Postmortem fetal brain pathology in P1 showed microencephaly, with a brain weight more than three standard deviations below the mean value for gestational weight (35 g), a thin cortex, and enlarged ventricles. At hematoxy-

(CM). The region between the red lines is homozygous in the three affected individuals and heterozygous in the unaffected sibling. (D) Electropherograms of DNA sequencing reactions, showing the *USP18* homozygote c.652C>T, p.Q218X mutation in P1, the heterozygous mutation in his father (identical to that of the mother and the healthy brother) and in P4 of family B, and the WT sequence of a healthy control (each repeated twice). (E) *USP18* expression before and after 24-h stimulation with IFN-β-1a in cultured fibroblasts from P1 and P2 (family A), P4 and P5 (family B), and three healthy controls (C1, C2, and C3) tested by quantitative RT-PCR using primers amplifying exon 4–6 of *USP18* (for primer sequences see Table S4) and normalized against the housekeeping gene *RNF111*. One unstimulated control is set as 1.0 on the y-axis, which allows fold-change comparison. Error bars, SD. RU, relative units. Cumulative data of two independent experiments under identical conditions. *, $P < 0.05$, unpaired Student's *t* test for each patient sample versus three controls.

lin and eosin (H&E) staining, there was irregular ependymal layering with curvilinear shape (Fig. 2 E, a), columnar arrangement, and focal erosion (Fig. 2 E, b), compared with age-matched control (Fig. 2 E, c). There were trajectories of polymicrogyria reflecting defective neuronal migration (Fig. 2 E, d). In the white matter, heterotopic neural cell clusters were observed. In the layers below the ependyme, areas of hemorrhage with hemosiderin-laden macrophages were observed (Fig. 2 E, e, f, and g), with lysis, rarefaction, necrosis, and dystrophic calcification in the germinal matrix areas, the white matter, and the cortex. We next stained the brains of the patient and control with markers for vessels (CD34), microglia (Iba-1), MHC class II (HLA-DR), and astrocytes (GFAP; Fig. 2 F). In the patient brain, there is a strong induction of the brain innate immune system, as indicated by the robust presence of astrocytes, microglia, and up-regulation of MHC class II molecules. Positive staining for phosphorylated STAT1 (pSTAT1) in the patient versus the control brain (Fig. 2 F, pSTAT1) was suggestive of activation of type I IFN pathway.

Enhanced induction of ISG transcripts in patient fibroblasts after IFN stimulation

USP18 functions as a negative feedback regulator of type 1 IFN signaling, down-regulating STAT-mediated ISG transcription. qRT-PCR was performed on cDNA from P1 and P2 and from control fibroblasts, with and without IFN-α stimulation, to determine the level of expression of several ISGs, *IFIT1*, *MX2*, and *ISG15*. Transcripts for the *IFIT1*, *MX2*, and *ISG15* were much more abundant in the cells of P1 and P2 than in those of controls after stimulation with IFN (Fig. 3, A–C). Next, we monitored the levels of phosphorylated STAT2 and of the ISG-encoded proteins MX1, IFIT1, USP18, and ISG15 in patient and control cells

Table 1. **Clinical data**

Characteristics	Family A			Family B (ref. Knoblauch)	
	P1	P2	P3	P4	P5
Sex	Female	Male	Male	Male	Male
Age at presentation	Antenatal (22 GW)	Day 1	Day 1	Antenatal	Antenatal
Born at GW	Termination of pregnancy	30 5/7	31 2/7	37	32
Timing of death	23 5/7 GW	1 wk	17 d	22 d	12 d
Head circumference	Small, no value	29 cm (+1 SD)	27.5 cm (0 SD)	33 cm (0 SD)	30.5 cm (+1 SD)
Birth weight	NA	1,600 g (−0 SD)	1,694 g (−0.5 SD)	2,300 g (−2 SD)	1,830 g (−1 SD)
Respiratory distress	NA	+ (no spontaneous respiration)	+ (ventilation within hours)	+ (ventilation within hours)	+ (no spontaneous respiration)
Seizures	NA	− (subclinical epileptic activity on EEG)	+	+	+
Brain MRI	Microcephaly	BS, BG, CBL, IV, P hemorrhage	P, CBL, BG hemorrhage	Massive cerebral hemorrhage	Periventricular signal intensities due to multiple small hemorrhages
	SC, BG, and PV calcification	No clear calcifications	No clear calcifications	Enlarged lateral ventricles	Septum pellucidum cyst, Cavum vergae, lack of gyration of temporal lobes, diminished gyration of parietal lobes
	Cortical destruction	Normal gyration	Cortical necrosis PV white matter abnormalities Loss of white/gray matter demarcation	Cerebellar hypoplasia Malformations BS and PF Brain CT: calcifications	
Thoracic x-ray	NP	Normal	Normal	Axillary calcifications, thin ribs, metaphyseal bands of humerus	Calcifications along M. sternocleidomastoideus, thin ribs
Abdominal ultrasound	NP	Normal	Ascites, abnormal renal cortex/parenchyma differentiation	NP	Hepatomegaly, pleural effusions
Cardiological examination	NP	PDA Bradycardia	ASD type II, PDA, Bradycardia, Widening of right and left coronary artery	NP	NP
Eye examination	NP	Normal	Thinning of retinal vessels	NP	Normal
Blood hematology/ chemistry	NA	Thrombocytopenia, SGOT/SGPT/ammonia and lactate elevation	SGOT/SGPT/ammonia and lactate elevation	Thrombocytopenia, Dyserythropoiesis on bone marrow aspiration	Thrombocytopenia

ASD, atrium septum defect; BG, basal ganglia; BS, brain stem; CBL, cerebellum; CT, computed tomography; GW, gestational week; IV, intraventricular; P, parenchymal; NA, not available; NP, not performed; PDA, persistent ductus arteriosus; PF, posterior fossa; PV, periventricular; SC, subcortical.

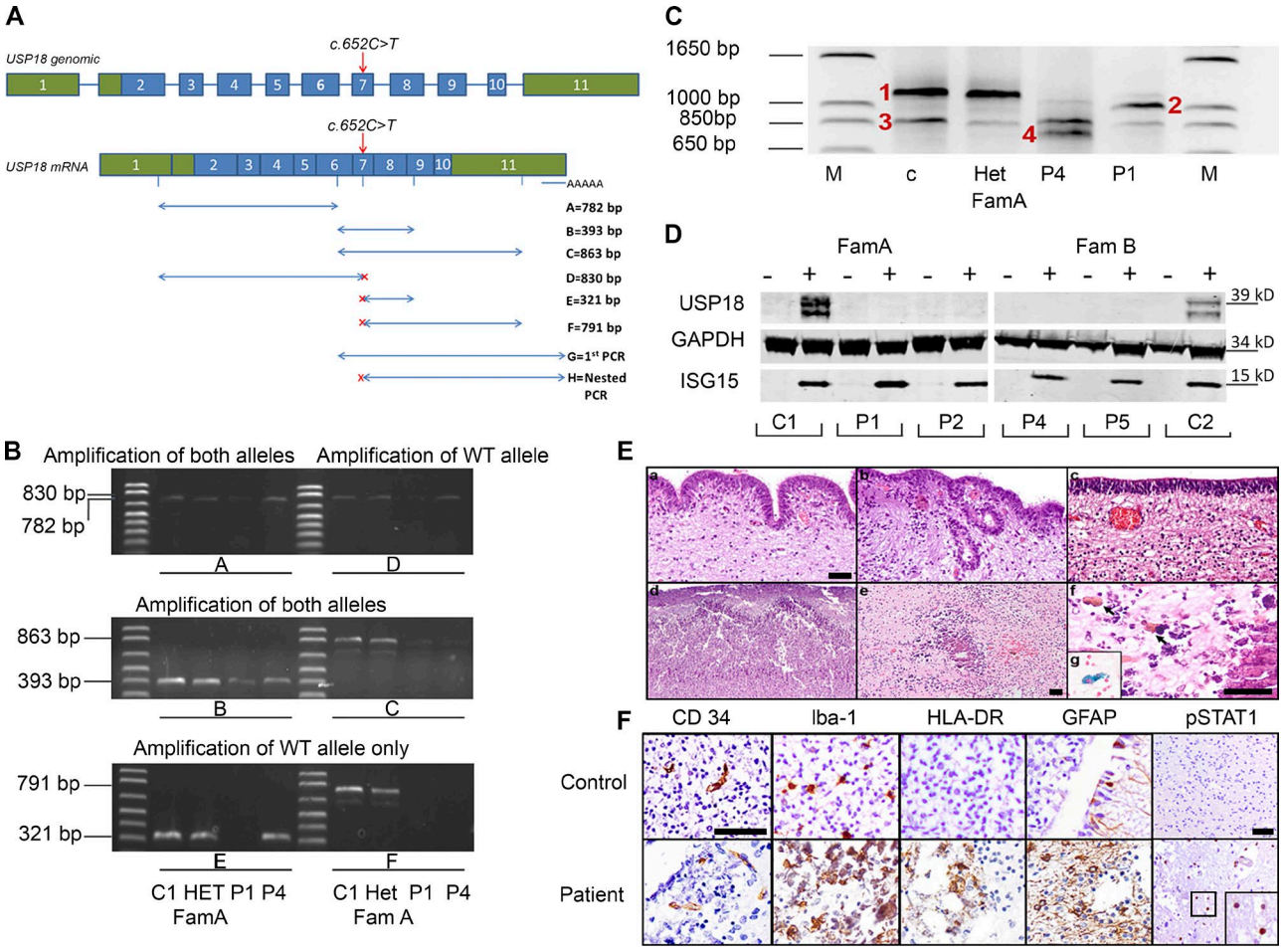

Figure 2. ***USP18* transcripts, protein, and brain pathology.** (A) Schematic of the genomic DNA and mRNA *USP18*, with coding regions in blue, UTRs in green, and the c.652C>T mutation indicated by the red arrow. RT-PCR primer locations and expected product sizes are shown from A to F in the key, and G and H refer to 3′ RACE and nested PCR primers, covering exon 1 to the poly-A tail. PCR primers designed to amplify only the c.652C WT allele are indicated by a red x. (B) RT-PCR amplicons obtained using the primer sets schematized in A. C1, control; Het-FamA, healthy heterozygote sibling from family A; P1, P1 from family A; P4, P4 from family B. Primers used are listed in Table S4. (C) Nested PCR products of the 3′ RACE cDNA amplification (area indicated in A, primer sets G and H). The four bands obtained in C1, P1, P4, and Het-FamA samples, indicated by red numbers, were subjected to capillary sequencing: band 1 (~1,200 bp), band 2 (~1,000 bp), band 3 (~850 bp), and band 4 (~800 bp). Both RT-PCR and 3′ RACE experiments were separately repeated three times with identical results. (D) Western blot analysis of the endogenous USP18 protein in cultured fibroblasts from controls and from P1, P2, P4, and P5, before and after stimulation for 24 h with IFN-β-1a. Levels of the IFN-inducible ISG15 protein and of GADPH as control were also measured. In control cells, IFN-induced USP18 and ISG15 were detected after IFNβ-1a treatment. In patients cells, no USP18 protein was detected. This experiment has been replicated twice with separate controls and with identical results. (E) H&E staining of autopsy brain material from P1. Irregular ependyme with a curvilinear shape, columnar arrangement (a), and numerous ependymal canals (b) are present, compared with an age-matched control case (c).Trajectories of polymicrogyria (d). Vessel-associated dystrophic calcifications in the white matter (e). (f) Magnification of e: with arrows showing hemosiderophages. (g) Prussian blue staining for iron. Bars: 50 µm (a and f), 100 µm (e); magnification in b and c is equal to a; magnification in d is equal to e. (F) P1 and age-matched control brain material. Immunohistochemistry for vessels (CD34) and for the presence of innate immune response activation in the white matter, using markers for the microglial ionized calcium-binding adaptor molecule 1 (Iba-1), MHC class II (HLA-DR), and the astrocyte marker glial fibrillary acidic protein (GFAP). pSTAT1 is used as marker for type I IFN response activation (inset showing a magnification of positive cells in the patient). Bars: (CD34 control) 50 µm (magnification in CD34, Iba-1, HLA-DR, and GFAP are equal to CD34 control); (pSTAT1 control) 50 µM (magnification in the patient is the same as in the control).

(Fig. 3 D). Persistent STAT2 phosphorylation and high levels of induced MX1 and IFIT1 proteins were detected in patients' cells as compared with WT controls. Analysis of the non–type I IFN-related gene product IL-6 showed no abnormal regulation (Fig. 3 E).

Transduction of patient fibroblasts with USP18 rescues the enhanced induction of ISGs and the increased global protein ISGylation

To ascertain that this enhanced type 1 IFN response with up-regulation of ISG expression was indeed caused by

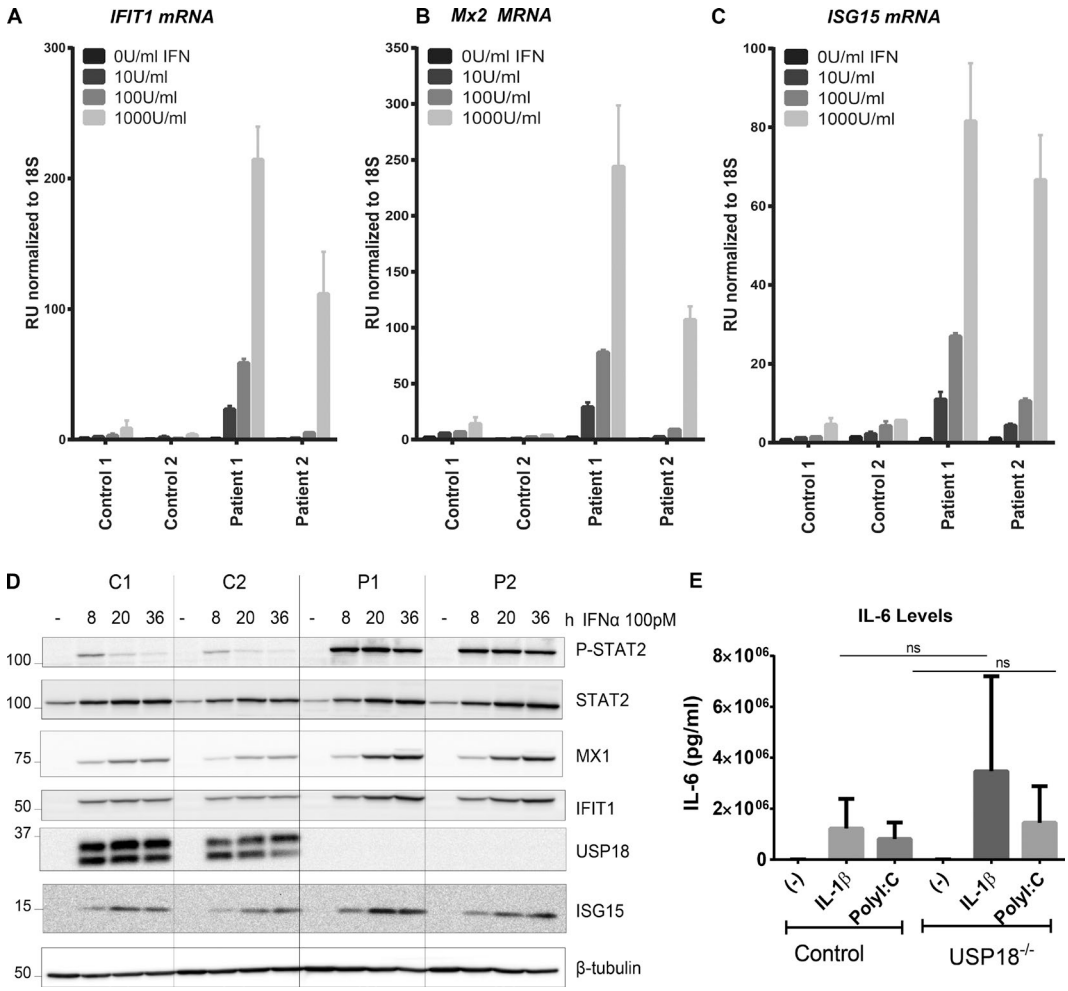

Figure 3. **mRNA and protein expression of *USP18* and ISGs, as assessed by qRT-PCR and Western blotting after IFN treatment, and IL-6 production assessment.** (A–C) Primary fibroblasts from C1 and C2 and from P1 and 2 were treated with the indicated doses of IFN-α2b for 12 h, washed with PBS, and left to rest for 36 h, after which relative mRNA levels were assessed for the genes indicated, with representative experiment of three with SD shown. (D) Primary fibroblasts from two controls (C1 and C2) and P1 and P2 were stimulated with 100 pM IFN-α2 for 8, 20, and 36 h. The levels of phosphorylated STAT2 and of the indicated ISG products were analyzed by Western blotting of 20 µg of cell lysate, representative experiment of two shown. RU, relative units. IL-6 production at 24 h after stimulation with 10 ng/ml IL-1B or 25 µg/ml Poly(I:C) was measured using ELISA. Shown are pooled data from two independent experiments, each done in duplicates using three different controls and two patient cell lines. Mann-Whitney test was used for statistical analyses, with SEM shown (E).

USP18 deficiency, we transduced USP18-deficient fibroblasts from P1 and P2 and control fibroblasts with lentiviral particles (LV)-expressing luciferase (Luc) or WT *USP18*. Unlike LV-Luc, LV-WT USP18 completely rescued the enhanced induction of ISGs at the mRNA level (Fig. 4, A–C). Similarly, at the protein level, unlike LV-Luc, LV-WT USP18 transduced patient fibroblasts exhibited reduced levels of phosphorylated STAT2, MX1, and IFIT1 (Fig. 4 D). ISGylated proteins are main targets of USP18 protease activity (Zhang and Zhang, 2011). We therefore determined global ISGylation levels and the amount of unconjugated ISG15. Consistently, fibroblasts from P1 and P2 stimulated with IFN-α displayed significantly greater amounts of ISGylated proteins than control cells (Fig. 4 E). As expected, LV-WT USP18 transduction, but not LV-Luc, decreased global protein ISGylation levels (Fig. 4 E). siRNA against *USP18*, but not control siRNA, in primary control fibroblasts completely phenocopied USP18-deficient cells when challenged with IFN (Fig. 4 F and G). Collectively, these rescue experiments indicate that the loss of USP18 is responsible for abnormal activation of IFN signaling. Moreover, our results demonstrate that, in humans, USP18-mediated regulation of IFN response is crucial for normal CNS development, and that its deficiency causes severe PTS. Yet, the diversity of phenotypes observed in the *Usp18*$^{-/-}$ mice of different genetic background likely reflects different basal levels of IFNs, which itself points to the contribution of additional genetic or epigenetic factors.

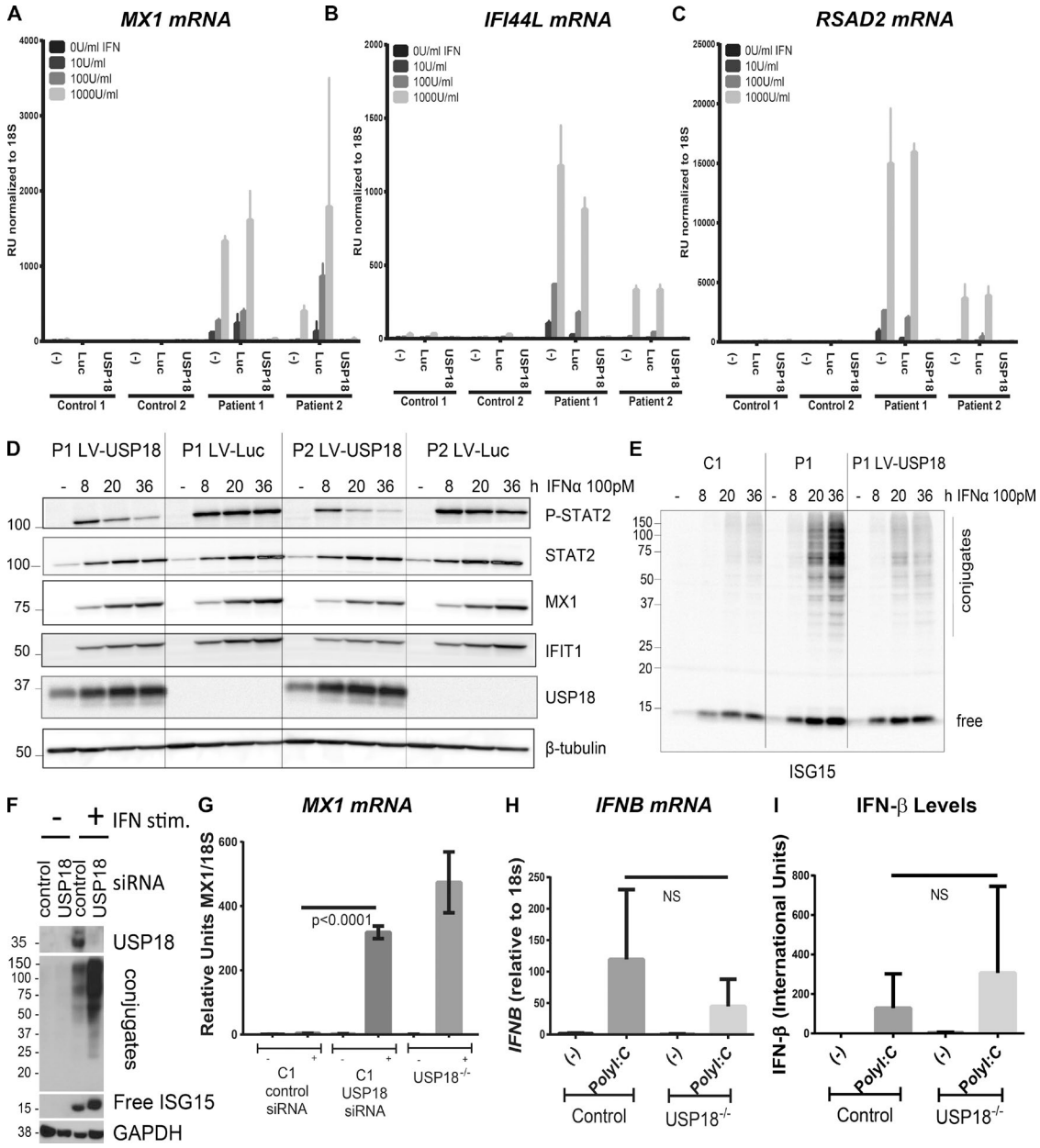

Figure 4. **WT *USP18* allele rescues USP18 deficiency.** Primary fibroblasts from C1 and C2 and from P1 and P2 were mock-transduced or transduced with luciferase-RFP or WT *USP18*, sorted, and treated with the indicated doses of IFN-α2b for 12 h, washed with PBS, and left to rest for 36 h, after which relative mRNA levels were assessed for the genes indicated (A–C) performed three times each with technical triplicates, representative experiment with SD shown. The levels of the indicated proteins were compared in fibroblasts from P1 and P2, transduced with *USP18* or with the control Luc LV. Cells were stimulated and processed as in Fig. 3 D, representative experiment of two shown (D). The levels of free and conjugated ISG15 were analyzed in lysates (40 µg/lane) from a control (C1), P1 (P1), and USP18-transduced fibroblasts from P1 (P1 LV-USP18), stimulated, and processed as described in Fig. 3 D, representative experiment of two are shown (E). Primary fibroblasts from C1 were transfected with either control siRNA or siRNA targeting *USP18*, followed by vehicle of IFN stimulation for 36 h, when USP18, GAPDH, free, and conjugated ISG15 were analyzed in lysates, representative of two experiments shown (F), or were primed or not for 12 h with 1,000 IU IFN along with P1 USP18$^{-/-}$ cells, followed by 36 h rest when *MX1* mRNA levels were assessed, representative of two experiments shown, performed in biological duplicates and technical triplicates. Student's *t* test was used for statistical analyses with SEM (G). *IFNB* mRNA expression was measured after a 4-h stimulation with 25 µg/ml Poly (I:C), as well as IFN-β production at 24 h, both in control and patient cells. Two control and patient cell lines, in triplicates in two independent experiments were used for mRNA measurements; three control and two patient cell lines, in triplicates in three independent experiments were used for IFN-β measurement. Mann-Whitney test was used for statistical analyses with SEM shown (H and I).

Notably, the brain pathology of USP18-deficient patients (Fig. 2 E, d) is similar to that observed in cases of congenital infection with neurotropic viruses, such as cytomegalovirus and lymphocytic choriomeningitis virus, with activation of meningeal and hematopoietic-derived macrophages and microglia and the induction of cytokines including type 1 IFN (Bale, 2009; Bonthius, 2012; Sakao-Suzuki et al., 2014). Our observations are consistent with previous studies suggesting that, in some congenital viral infections, the brain damage may owe as much to the host response as to the infectious agent itself (Gresser et al., 1980). This is crucial for future considerations on management of congenital infections, as targeting only the virus itself will not be sufficient to avoid permanent damage to the fetus.

Interestingly, the mechanism behind type I interferonopathies described to date in AGS differs from the one operating in USP18 deficiency, as type I IFN dysregulation in USP18 deficiency is not a result of aberrant induction of these cytokines but is caused by an aberrant response to type I IFN. In support of this, although body fluids of the patients were not stored, IFNB mRNA and protein level were comparable to controls when patient cells were stimulated with Poly (I:C; Fig. 4, H and I).

Human ISG15 deficiency leads to milder USP18 dysfunction and causes cerebral abnormalities compatible with adult life, such as basal ganglia calcification and occasional seizures (Zhang et al., 2015). The cells of ISG15-deficient patients demonstrated reduced, albeit still detectable, amounts of USP18, and displayed defective down-regulation of type 1 IFN signaling. We speculate that biallelic hypomorphic *USP18* mutations (i.e., leading to residual protein function) may cause milder cerebral abnormalities with prolonged survival, possibly overlapping the phenotypic spectrum of *ISG15* mutations. Therapeutically, USP18 represents an attractive target, with agonists being of use in clinical settings where there is overabundance of type I IFNs and USP18 antagonists acting to prolong the beneficial effects of therapeutic IFNs, as in multiple sclerosis, hairy cell leukemia, and melanoma. Likewise, in genetic counseling and prenatal diagnosis of severe perinatal PTS, *USP18* should be added to the list of genes to be tested. Collectively, our results establish USP18 deficiency as a novel genetic cause of severe PTS.

MATERIALS AND METHODS

Ethics approval. Written parental consent was obtained. Genetic tests were performed according to The Erasmus University Medical Center's local ethics board approved protocol MEC-2012387.

Linkage analysis. Linkage analysis was performed on Illumina CytoSNP12v2.1 array data for the three affected siblings, their healthy brother, and both parents of family A. Genotype data were available for >300,000 SNPs per individual. Linkage analysis was performed with Merlin v1.0.1 (in the Easy Linkage Plus v5.08 package). An autosomal recessive model was specified, with an estimated allele frequency of 0.0001 and 100% penetrance. Closely spaced SNP markers were used for the analysis, so the genome analysis was performed with predefined spacings of 0.1 and 0.15 cM. Genomic regions with LOD scores >2.5 were considered to be candidate intervals. Haplotypes were constructed and graphic visualizations were performed with HaploPainter v029.5 (Hoffmann and Lindner, 2005) to facilitate inspection and analysis.

Whole-exome sequencing. Whole-exome sequencing was performed on DNA extracted from the fibroblasts of P1 and peripheral leukocytes from the parents and P2 and P3 of family A with the Sure Select All Exome V4 capture kit (Agilent) on a HiSeq2000 machine (Illumina). The statistics are provided in Table S1. BWA version 0.5.9 (Li and Durbin, 2009) and NARWHAL software (Brouwer et al., 2012) were used to align reads with the reference genome (hg19). Variants were called with GATK (version 1.2–29; McKenna et al., 2010) and SAMtools (version 0.1.13). Variants were annotated with ANNOVAR software (revision 511; Wang et al., 2010) and filtered with TIBCO Spotfire version 4.5 (Tables S1 and S2).

Light microscopy and immunohistochemistry. Brain autopsy material was fixed in 4% paraformaldehyde and embedded in paraffin. Sections (4 µm thick) were cut and stained with H&E or Prussian blue, for iron visualization. Immunohistochemical staining was performed with a biotin-avidin and alkaline phosphatase/anti-alkaline phosphatase visualization. The primary antibodies used were as follows: anti-CD3 (T cells, rat monoclonal antibody; Serotec), anti-glial fibrillary acidic protein (anti-GFAP, rabbit polyclonal antibody; Dako), anti–HLA-DR (MHC class II, mouse monoclonal antibody, clone LN3; eBioscience), antiionized calcium-binding adaptor molecule (Iba)-1 antibody (microglia, macrophages; Wako), anti-CD34 (vessels, clone B-C34; Cell Sciences), and anti-pSTAT1 (clone 58D6, #9167; Cell Signaling Technology). The pictures were taken with a BZ-9000 Biorevo microscope (Keyence; Neu-Isenburg)

Sanger sequencing of missing exons in linked area and USP18. PCR and Sanger sequencing were conducted according to standard methods. The Sanger sequencing of *USP18* was complicated by the presence of a pseudogene with a very similar sequence, *USP41*. Fig. S3 shows the alignment of these two genes, highlighting their similarity. Table S3 lists the exons for which there was little or no coverage, together with the primers used for Sanger sequencing. Table S4 lists the genomic primers for Sanger sequencing of *USP18*.

qRT-PCR. qRT-PCR was performed with a KAPA SYBR FAST qPCR kit (Kapa Biosystems) in the CFX96 Real-Time system (Bio-Rad Laboratories). Thermal cycling conditions were as follows: denaturation (95°C for 3 min), followed by

35 cycles of denaturation (95°C for 5 min), annealing, and extension (60°C for 30 min). Fluorescence detection and data analysis were performed with CFX Manager 2.0 (Bio-Rad Laboratories). Experiments were performed in triplicate, with *RNF111* (Entrez Gene ID 54778 [OMIM 605840]) as the reference gene for the normalization of expression data (Bustin et al., 2009) and *COPS5* (Entrez Gene ID 10987 [OMIM 604850]) as a secondary housekeeping gene. The primers used are also listed in Table S4. For qRT-PCR after transduction, see Stimulation and qRT-PCR.

Fibroblast culture, cDNA synthesis, and RT-PCR. Fibroblasts were routinely tested for mycoplasma infection and were cultured in 75-cm^2 culture flasks, in DMEM, to 80% confluence. Total RNA was extracted on RNeasy mini columns (QIA GEN) according to the manufacturer's protocol. Reverse transcription was performed on 1 µg of RNA in a total volume of 20 µl, with the iScript cDNA Synthesis kit (Bio-Rad Laboratories) used according to the manufacturer's instructions (Poulton et al., 2011). RT-PCR was performed using FASTStart Taq DNA polymerase (Sigma-Aldrich) according to manufacturer's instructions. Primers for RT-PCR analysis for the experiments shown in Fig. 2 B are listed in Table S4.

3′ RACE PCR. Total RNA from control and patients fibroblasts was isolated using TRIzol (Ambion). 3′ RACE PCR was performed using the 3′ RACE System for Rapid Amplification of cDNA ends (Invitrogen), according to the manufacturer's instruction.

3′ RACE Universal Amplification Primer (UAP), supplied in the kit, complementary to the adaptor primer, and a gene-specific primer designed in exon 6 of USP18 (5′-CAGAAACAGCAGCATGCTCACC-3′) were used for first amplification, followed by nested PCR with the UAP and a second gene-specific primer designed in exon 7 of USP18 (5′-CGCCCTGCACTGCTTCTTCC-3′).

Stimulation of fibroblasts with interferon. Fibroblasts were stimulated for 12 or 24 h at 37°C with either 110 U/ml human IFN-β-1a (11415–1; pbl interferon source) or 10–1,000 U/ml IFN-α-2b (Merck IntronA) in complete medium. The IFN was removed by thorough washing with PBS, and the cells were either harvested or allowed to rest for 36 h at 37°C in normal growth medium. Cells were harvested for RNA isolation.

Western blot analysis and siRNA experiments. In Fig. 2 C, cell pellets were resuspended in a previously described buffer (Francois-Newton et al., 2012; 50 mM Tris/HCl, pH 8.0, 150 mM NaCl, 1% Triton X100, 0.5% sodium deoxycholate, 0.03% SDS, and 1 mM Na_3VO_4). We ran 40 µg of total protein on a precast Criterion XT 4–12% bis Tris gel (Bio-Rad Laboratories). The blots were incubated with anti-USP18 (1:1,000; rabbit monoclonal; Cell Signaling Technology #4813; recognizing residues surrounding amino acid Pro45), anti-ISG15 (1:500, rabbit polyclonal), or anti-GAPDH (mouse 1:1,000; monoclonal; Li-Cor Biosciences) primary antibodies; 680 nm goat anti–rabbit and 800 nm goat anti–mouse conjugates were used as secondary antibodies. In Figs. 3 C and 4 (D and E), cell lysates were prepared in modified RIPA buffer (50 mM Tris-HCl, pH 8.0, 200 mM NaCl, 1% NP-40, 0.5% DOC, 0.05% SDS, and 2 mM EDTA) with 1 mM Na_3VO_4 and a cocktail of proteases inhibitors (Roche). Rec IFN-α2 was provided by D. Gewert (Wellcome Trust, London, England). We used antibodies against STAT2 (EMD Millipore), phosphorylated Tyr689 STAT2 (EMD Millipore), USP18 (Cell Signaling Technology), β-tubulin (Takara Bio Inc.), ISG15 (gift from E.C. Borden, Cleveland Clinic, Cleveland, OH), IFIT1 (gift from G. Sen, Cleveland Clinic, Cleveland, OH), and Mx1 (MxA; gift from O. Haller, University of Freiburg, Freiburg, Germany). Signal was detected with enhanced chemiluminescence detection reagent (Western Lightning; PerkinElmer) and acquired with a Fuji ImageQuant LAS-4000 machine. Control primary human fibroblasts were silenced by incubation for 24 h with 25 nM *USP18*-siRNA (Dharmacon; pool-siRNA), followed by priming with IFN. siRNA transfections were performed with Lipofectamine RNAi max reagent (Invitrogen) according to the manufacturer's instructions.

Transduction. Lentiviral particles were produced by transfecting HEK-293T cells, in the presence of Lipofectamine-2000 (Invitrogen), with the following constructs: pCAGGS-VSV-G, pCMV-Gag/Pol, and pTRIP-hUSP18-IRES-RFP or pTRIP-luciferase-IRES-RFP. Supernatants were collected 36 h after transfection and clarified by centrifugation. The fibroblasts were covered with lentiviral inoculum and incubated at 37°C. Supplemental growth medium was added, and transduction efficiency was checked by fluorescence microscopy. Transduced fibroblasts were sorted (FACS Aria II; BD) into (−), low (Lo), medium (Med), and high (Hi) expression groups on the basis of RFP expression. We focused on the Lo expression group. Transduced cell populations were expanded and grown in the same conditions as untransduced cells, and the level of transduced gene expression was periodically confirmed by fluorescence microscopy.

Stimulation and qRT-PCR. Untransduced luciferase- and USP18-transduced fibroblasts were treated with 0 U/ml (mock), 10 U/ml, 100 U/ml, or 1,000 U/ml interferon α-2b (Merck IntronA) in normal growth medium for 12 h at 37°C. The IFN was removed by thorough washes with PBS, and the cells were allowed to rest for 36 h at 37°C in normal growth medium. The cells were then lysed and RNA was extracted with a kit, according to the manufacturer's instructions (RNeasy; QIAGEN). RNA was reverse-transcribed according to the enzyme manufacturer's instructions (ABI High Capacity Reverse transcription). The relative expression levels of multiple IFN-stimulated genes (ISGs; *MX1*, *MX2*, *RSAD2*, *ISG15*, *IFI44L*, and *IFIT1*) were analyzed by TaqMan quanti-

tative real-time PCR on technical duplicates (TaqMan Universal Master Mix II w/UNG; LightCycler 480 II; Roche). The relative expression of the ISGs was calculated by the ΔΔCT method, with comparison to the mean value for the untreated controls.

Online supplemental material. Fig. S1 shows linkage data and haplotyping. Fig. S2 shows CG control alleles. Fig. S3 shows alignment of USP18 and USP41. Table S1 shows exome sequencing data. Table S2 lists filtering steps for family A. Table S3 lists the exons for which there was little or no coverage, together with the primers used for Sanger sequencing. Table S4 lists the genomic primers for Sanger sequencing of *USP18*. Table S5 lists haplotypes of chromosome 22q11 in family A and B using Illumina cyto-snp-850 kb arrays. Clinical data from family A is provided as supplemental text. Online supplemental material is available at http://www.jem.org/cgi/content/full/jem.20151529/DC1.

ACKNOWLEDGMENTS

We thank Dr. Peter van der Spek for sharing the whole genome sequencing control data and Dr. Kathleen Millen (University of Washington, Seattle, WA) for helpful discussions. We also thank Tom de Vries Lentsch for the graphical work and Julie Sappa for copyediting the manuscript.

Financial support was obtained by NutsOhra Funds project 1203-030 to G.M.S. Mancini. D. Bogunovic is supported by the National Institute of Allergy and Infectious Diseases grant number R00AI106942-02. Z. Li and S. Pellegrini acknowledge institutional support from Institut Pasteur, Centre National de la Recherche Scientifique, and Institut National de la Santé et de la Recherche Médicale. Y.J. Crow acknowledges the European Research Council (GA 309449).

The authors declare no competing financial interests.

Submitted: 22 September 2015
Accepted: 17 May 2016

REFERENCES

Bale, J.F. Jr. 2009. Fetal infections and brain development. *Clin. Perinatol.* 36:639–653. http://dx.doi.org/10.1016/j.clp.2009.06.005

Bonthius, D.J. 2012. Lymphocytic choriomeningitis virus: an underrecognized cause of neurologic disease in the fetus, child, and adult. *Semin. Pediatr. Neurol.* 19:89–95. http://dx.doi.org/10.1016/j.spen.2012.02.002

Brouwer, R.W., M.C. van den Hout, F.G. Grosveld, and W.F. van Ijcken. 2012. NARWHAL, a primary analysis pipeline for NGS data. *Bioinformatics.* 28:284–285. http://dx.doi.org/10.1093/bioinformatics/btr613

Bustin, S.A., V. Benes, J.A. Garson, J. Hellemans, J. Huggett, M. Kubista, R. Mueller, T. Nolan, M.W. Pfaffl, G.L. Shipley, et al. 2009. The MIQE guidelines: minimum information for publication of quantitative real-time PCR experiments. *Clin. Chem.* 55:611–622. http://dx.doi.org/10.1373/clinchem.2008.112797

Crow, Y.J. 2015. Type I interferonopathies: mendelian type I interferon up-regulation. *Curr. Opin. Immunol.* 32:7–12. http://dx.doi.org/10.1016/j.coi.2014.10.005

Crow, Y.J., and J.L. Casanova. 2014. STING-associated vasculopathy with onset in infancy--a new interferonopathy. *N. Engl. J. Med.* 371:568–571. http://dx.doi.org/10.1056/NEJMe1407246

Crow, Y.J., and J. Rehwinkel. 2009. Aicardi-Goutieres syndrome and related phenotypes: linking nucleic acid metabolism with autoimmunity. *Hum. Mol. Genet.* 18(R2):R130–R136. http://dx.doi.org/10.1093/hmg/ddp293

Donley, D.K. 1993. TORCH infections in the newborn. *Semin. Neurol.* 13:106–115. http://dx.doi.org/10.1055/s-2008-1041114

Fine, J.D., and K.A. Arndt. 1985. The TORCH syndrome: a clinical review. *J. Am. Acad. Dermatol.* 12:697–706. http://dx.doi.org/10.1016/S0190-9622(85)70095-3

Francois-Newton, V., M. Livingstone, B. Payelle-Brogard, G. Uzé, and S. Pellegrini. 2012. USP18 establishes the transcriptional and anti-proliferative interferon α/β differential. *Biochem. J.* 446:509–516. http://dx.doi.org/10.1042/BJ20120541

Goldmann, T., N. Zeller, J. Raasch, K. Kierdorf, K. Frenzel, L. Ketscher, A. Basters, O. Staszewski, S.M. Brendecke, A. Spiess, et al. 2015. USP18 lack in microglia causes destructive interferonopathy of the mouse brain. *EMBO J.* 34:1612–1629. http://dx.doi.org/10.15252/embj.201490791

Gresser, I., L. Morel-Maroger, Y. Rivière, J.C. Guillon, M.G. Tovey, D. Woodrow, J.C. Sloper, and J. Moss. 1980. Interferon-induced disease in mice and rats. *Ann. N.Y. Acad. Sci.* 350(1 Regulatory Fu):12–20. http://dx.doi.org/10.1111/j.1749-6632.1980.tb20602.x

Hoffmann, K., and T.H. Lindner. 2005. easyLINKAGE-Plus--automated linkage analyses using large-scale SNP data. *Bioinformatics.* 21:3565–3567. http://dx.doi.org/10.1093/bioinformatics/bti571

Knoblauch, H., C. Tennstedt, W. Brueck, H. Hammer, T. Vulliamy, I. Dokal, R. Lehmann, F. Hanefeld, and S. Tinschert. 2003. Two brothers with findings resembling congenital intrauterine infection-like syndrome (pseudo-TORCH syndrome). *Am. J. Med. Genet. A.* 120A:261–265. http://dx.doi.org/10.1002/ajmg.a.20138

Konradt, C., and C.A. Hunter. 2015. Immune-mediated viral clearance from the CNS without collateral damage. *J. Exp. Med.* 212:1141–1142. http://dx.doi.org/10.1084/jem.2128insight3

Lander, E., and L. Kruglyak. 1995. Genetic dissection of complex traits: guidelines for interpreting and reporting linkage results. *Nat. Genet.* 11:241–247. http://dx.doi.org/10.1038/ng1195-241

Li, H., and R. Durbin. 2009. Fast and accurate short read alignment with Burrows-Wheeler transform. *Bioinformatics.* 25:1754–1760. http://dx.doi.org/10.1093/bioinformatics/btp324

Liu, Y., A.A. Jesus, B. Marrero, D. Yang, S.E. Ramsey, G.A. Montealegre Sanchez, K. Tenbrock, H. Wittkowski, O.Y. Jones, H.S. Kuehn, et al. 2014. Activated STING in a vascular and pulmonary syndrome. *N. Engl. J. Med.* 371:507–518. http://dx.doi.org/10.1056/NEJMoa1312625

Malakhova, O.A., K.I. Kim, J.K. Luo, W. Zou, K.G. Kumar, S.Y. Fuchs, K. Shuai, and D.E. Zhang. 2006. UBP43 is a novel regulator of interferon signaling independent of its ISG15 isopeptidase activity. *EMBO J.* 25:2358–2367. http://dx.doi.org/10.1038/sj.emboj.7601149

McKenna, A., M. Hanna, E. Banks, A. Sivachenko, K. Cibulskis, A. Kernytsky, K. Garimella, D. Altshuler, S. Gabriel, M. Daly, and M.A. DePristo. 2010. The Genome Analysis Toolkit: a MapReduce framework for analyzing next-generation DNA sequencing data. *Genome Res.* 20:1297–1303. http://dx.doi.org/10.1101/gr.107524.110

Meuwissen, M.E., D.J. Halley, L.S. Smit, M.H. Lequin, J.M. Cobben, R. de Coo, J. van Harssel, S. Sallevelt, G. Woldringh, M.S. van der Knaap, et al. 2015. The expanding phenotype of COL4A1 and COL4A2 mutations: clinical data on 13 newly identified families and a review of the literature. *Genet. Med.* 17:843–853. http://dx.doi.org/10.1038/gim.2014.210

Poulton, C.J., R. Schot, S.K. Kia, M. Jones, F.W. Verheijen, H. Venselaar, M.C. de Wit, E. de Graaff, A.M. Bertoli-Avella, and G.M. Mancini. 2011. Microcephaly with simplified gyration, epilepsy, and infantile diabetes linked to inappropriate apoptosis of neural progenitors. *Am. J. Hum. Genet.* 89:265–276. http://dx.doi.org/10.1016/j.ajhg.2011.07.006

Reardon, W., A. Hockey, P. Silberstein, B. Kendall, T.I. Farag, M. Swash, R. Stevenson, and M. Baraitser. 1994. Autosomal recessive congenital intrauterine infection-like syndrome of microcephaly, intracranial

calcification, and CNS disease. *Am. J. Med. Genet.* 52:58–65. http://dx.doi.org/10.1002/ajmg.1320520112

Rice, G.I., P.R. Kasher, G.M. Forte, N.M. Mannion, S.M. Greenwood, M. Szynkiewicz, J.E. Dickerson, S.S. Bhaskar, M. Zampini, T.A. Briggs, et al. 2012. Mutations in ADAR1 cause Aicardi-Goutières syndrome associated with a type I interferon signature. *Nat. Genet.* 44:1243–1248. http://dx.doi.org/10.1038/ng.2414

Ritchie, K.J., M.P. Malakhov, C.J. Hetherington, L. Zhou, M.T. Little, O.A. Malakhova, J.C. Sipe, S.H. Orkin, and D.E. Zhang. 2002. Dysregulation of protein modification by ISG15 results in brain cell injury. *Genes Dev.* 16:2207–2212. http://dx.doi.org/10.1101/gad.1010202

Sakao-Suzuki, M., H. Kawasaki, T. Akamatsu, S. Meguro, H. Miyajima, T. Iwashita, Y. Tsutsui, N. Inoue, and I. Kosugi. 2014. Aberrant fetal macrophage/microglial reactions to cytomegalovirus infection. *Ann. Clin. Transl. Neurol.* 1:570–588. http://dx.doi.org/10.1002/acn3.88

Shin, Y.H., L. Glass, and H.E. Evans. 1976. The "torch" syndrome. *Pediatr. Ann.* 5:106–113. http://dx.doi.org/10.3928/0090-4481-19760201-11

Vivarelli, R., S. Grosso, M. Cioni, P. Galluzzi, L. Monti, G. Morgese, and P. Balestri. 2001. Pseudo-TORCH syndrome or Baraitser-Reardon syndrome: diagnostic criteria. *Brain Dev.* 23:18–23. http://dx.doi.org/10.1016/S0387-7604(00)00188-1

Wang, K., M. Li, and H. Hakonarson. 2010. ANNOVAR: functional annotation of genetic variants from high-throughput sequencing data. *Nucleic Acids Res.* 38:e164. http://dx.doi.org/10.1093/nar/gkq603

Zhang, D., and D.E. Zhang. 2011. Interferon-stimulated gene 15 and the protein ISGylation system. *J. Interferon Cytokine Res.* 31:119–130. http://dx.doi.org/10.1089/jir.2010.0110

Zhang, X., D. Bogunovic, B. Payelle-Brogard, V. Francois-Newton, S.D. Speer, C. Yuan, S. Volpi, Z. Li, O. Sanal, D. Mansouri, et al. 2015. Human intracellular ISG15 prevents interferon-α/β over-amplification and auto-inflammation. *Nature.* 517:89–93. http://dx.doi.org/10.1038/nature13801